BIOCELL
2021 45(3): 685-694

Tech Science Press

RPA3 is transcriptionally activated by YY1 and its depletion enhances radiosensitivity of triple-negative and HER2-positive breast cancer

Yanfei LI[1]; Lulu DAI[2]; Ke CAI[2]; Yingkui SONG[2]; Xiqing LIU[3,*]

[1] Clinical Laboratory, Laiyang Central Hospital of Yantai, Laiyang, 265200, China
[2] Department of General Surgery, The Eighth People's Hospital of Qindao, Qingdao, 266000, China
[3] Hepatobiliary Surgery, Anqiu People's Hospital, Anqiu, 262100, China

Key words: RPA3, YY1, Breast cancer, Radiotherapy

Abstract: RPA3 (Replication Protein A3) (14 kD) is a part of the canonical heterotrimeric replication protein A complex (RPA/RP-A). This study aimed to explore the functional role of RPA3 and the mechanisms of its dysregulation in breast cancer. Data from the Cancer Genome Atlas (TCGA)-breast cancer patients and GSE75688 were utilized for gene expression and survival analysis. Breast cancer cell lines MDA-MB-231 and SK-BR-3 were used for in-vitro cell studies. Clonogenic assay and immunofluorescent staining of γ-H2AX were performed to examine radiation-induced cytotoxicity. Systemic correlation analysis was performed to identify potential transcription factors (TFs) regulating RPA3 expression. ChIP-qPCR and dual-luciferase assay were conducted to verify the transcriptional activating effect of YY1 on RPA3 expression. Bioinformatic analysis showed that RPA3 expression was upregulated in breast cancer. Its upregulation was associated with poor survival of basal-like and HER2+ cases. RPA3 inhibition by siRNA reduced colony formation and increased γ-H2AX foci formation after irradiation in MDA-MB-231 and SK-BR-3 cells. RPA3 expression was transcriptionally activated by YY1 via promoter binding in the two cell lines. Both RPA3 and YY1 expression were positively correlated with their gene-level copy numbers. RPA3 might serve as a potential target for radio-sensitization in basal-like and HER2+ breast cancer.

Introduction

Breast cancer is a group of heterogeneous diseases with distinct genetic features, epigenetic alterations, pathobiological behaviors, responses to therapy, and clinical prognosis (Chung *et al.*, 2017; Vlashi *et al.*, 2014). The 50-gene qPCR assay (PAM50) revealed that breast cancers can be classified into five molecular groups, namely luminal A, luminal B, human epidermal growth factor receptor 2 (HER2)-positive ($HER2^+$), basal-like, and normal-like (Nielsen *et al.*, 2014). Although the molecular subtyping provided valuable information for chemotherapy, endocrine therapy and targeted therapy, the value of PAM50 subtypes in radiotherapy has not been well-characterized in clinical practice (He *et al.*, 2018). Currently, radiotherapy is still an important tool with multiple utilizations in breast cancer therapy, including radiation after breast-conserving surgery; prophylactic irradiation for high-risk patients after mastectomy; radiation for advanced cancers when surgery is not feasible; radiation for local recurrence, and palliative radiotherapy for distant metastases (He *et al.*, 2018). However, some patients may not benefit from this treatment due to individual variations in radiosensitivity (Langlands *et al.*, 2013). Therefore, it is necessary to understand the mechanisms leading to chemoresistance for the future development of radio-sensitizers.

RPA3 (Replication Protein A3) (14 kD) is one of the components of the canonical heterotrimeric replication protein A complex (RPA/RP-A), together with RPA1 (70 kD) and RPA2 (32kD) (Lin *et al.*, 1998). This complex binds to and stabilizes single-stranded DNA (ssDNA) intermediates during DNA replication or in response to DNA damage. It also recruits and activates a series of protein complexes for homologous recombination (HR) repair, such as ataxia-telangiectasia mutated- and Rad3-related interacting protein (ATRIP) (Marechal *et al.*, 2014; Zou and Elledge, 2003), DNA repair protein RAD51 and RAD52 (Aboussekhra *et al.*, 1995) and HepA-related protein (HARP) (Yusufzai *et al.*, 2009). DNA repair capability of tumor cells is negatively correlated with their radiosensitivity (Glanzer *et al.*, 2014). Targeting HR repair

*Address correspondence to: Xiqing Liu, lxqsjrlfs2008@163.com
Received: 13 August 2020; Accepted: 03 December 2020

Doi: 10.32604/biocell.2021.013612

has been considered a strategy for chemo/radiotherapy sensitization (Peng *et al.*, 2014). Aberrant *RPA3* expression was observed in gastric cancer, hepatocellular carcinoma, nasopharyngeal carcinoma, and also might serve as a prognostic biomarker (Dai *et al.*, 2017; Qu *et al.*, 2017; Xiao *et al.*, 2018). Inhibiting *RPA3* expression can enhance the radiosensitivity of hepatocellular carcinoma (Luo *et al.*, 2019) and nasopharyngeal carcinoma (Qu *et al.*, 2017). However, the expression profile of *RPA3* and its functional role in the radiosensitivity of breast cancer have not been identified yet.

In this study, we aimed to explore the expression profiles of *RPA3* and its prognostic value in breast cancer. Then, we studied its functional role in regulating the radiosensitivity of basal-like and $HER2^+$ breast tumor cells. Systemic screening of transcription factors identified YY1 as a high potential regulator of *RPA3* expression. YY1 has been characterized as an important TF upregulated in breast cancer and regulates the malignant transformation of breast cancer (Lu *et al.*, 2019). Therefore, we further explored whether YY1 regulates *RPA3* transcription.

Materials and Methods

Data extraction from Genotype-Tissue Expression (GTEx) and The Cancer Genome Atlas-Breast Cancer (TCGA-BRCA)

The RNA-seq data from normal mammary tissues were acquired from the GTEx (Consortium, 2013), while RNA-seq data from breast cancer and adjacent (adj.) normal tissues were obtained from TCGA-BRCA. Data acquisition was performed using the UCSC Xena (http://xena.ucsc.edu/) (Goldman *et al.*, 2020). PAM50 subtypes (determined by RNA-seq data), tumor gene-level copy number alterations (CNAs, delete germline copy number variation), survival data, including progression-free survival (PFS), and disease-specific survival (DSS), were also extracted.

Survival analysis using Kaplan-Meier Plotter

Kaplan-Meier Plotter (http://kmplot.com) was used to check recurrence-free survival (RFS) data integrated from microarray data of 1809 breast cancer patients (Gyorffy *et al.*, 2010). Kaplan-Meier survival curves were generated by the median or optimal cutoff of *RPA3* expression.

Single-cell transcriptional data and functional states in breast cancer cells

The association between *RPA3* expression and the functional states of breast cancer cells at the single-cell level was assessed using the CancerSEA platform (http://biocc.hrbmu.edu.cn/CancerSEA/home.jsp), which provides an analytic strategy to determine the correlation between gene expression and 14 functional states of cancer cells (Yuan *et al.*, 2019). These states were estimated according to the gene-expression profile at the single-cell level, using the signatures from Gene Ontology, MSigDB, Cyclebase, HCMDB and StemMapper. The state activity scores were calculated using the Gene Set Variation Analysis (GSVA) (Yuan *et al.*, 2019). The tumor cell data from basal-like (N = 130) and $HER2^+$ (N = 89) cases in one previous single-cell RNA-seq dataset (GSE75688) (Chung *et al.*, 2017) were retrieved for analysis.

Transcription factor (TF) data retrieved from JASPAR

TF gene list was collected from the JASPAR database (http://jaspar.genereg.net/) (Stormo, 2013). The promoter segment of *RPA3* was acquired by checking the promoter clone of human *RPA3* (#HPRM44615, Genome = hg38; chr7-:7719949-7718330; TSS = 7718607) in Genecopoeia. The promoter segment was scanned in JASPAR to identify potential YY1 binding sites by setting the relative profile score threshold to 90%.

Cell culture and treatment

Basal-like representative MDA-MB-231 and $HER2^+$ representative SK-BR-3 human breast cancer cell lines were purchased from the Cell Resource Center, Institute of Basic Medical Sciences, Chinese Academy of Medical Sciences (Beijing, China). These two cell lines were maintained in Dulbecco's modified eagle medium (DMEM) (Lonza, Walkersville, MD, USA) at 37°C in a 90% humidified incubator, with 5% CO_2.

Gene knockdown

Small interfering RNA (siRNA) and scramble controls were synthesized by General Biosystem (Chuzhou, Anhui, China), with the following sequences: *RPA3* siRNA (#1, 5'-CCGGCAUGCUAGCUCAAUUTT-3'; #2, 5'-GCAUGCUAGCUCAAUUCAUTT-3', #3, 5'-GCCACCAUCUUGUGUACAUTT-3') and scramble: 5'-GCUAUGCUCGCAUAUCACUTT-3'; *YY1* siRNA (#1, 5'-CCAAACAACUGGCAGAAUUTT-3'; #2, 5'-GCUCCAAGAACAAUAGCUUTT-3', #3, 5'-CCCAAACAACUGGCAGAAUTT-3') and scramble: 5'-CACACGACUGACAAGCAUATT-3'. Traditional forward transfection was conducted. Briefly, cells were seeded into a six-well plate at a density of 1×10^6 cells per well for 24 h at 37°C. Then, the cells were transfected with the siRNAs (50 nM), using Lipofectamine 2000 (Thermo Fisher Scientific, Waltham, MA, USA) according to the manufacturer's instructions.

Real-time quantitative RT-PCR (RT-qPCR)

Total RNA was extracted from cells using the High Pure RNA Isolation Kit (Roche Applied Science, Mannheim, Germany). Then, total RNA was reversely transcribed into cDNA using the first-strand cDNA synthesis kit (Roche Applied Science) according to the manufacturer's instructions. Real-time qPCR was then performed as described previously (Tuo *et al.*, 2015). The sense and antisense primers for gene amplification were: *RPA3*, 5'-AAGCCTGTCTGCTTCGTAGGGA-3' and 5'-CGGTTACTCTTCCAACCACTTCC-3', *YY1*, 5'-GGAGGAATACCTGGCATTGACC-3' and 5'-CCCTGAACATCTTTGTGCAGCC-3'. The relative expression level of mRNA was evaluated by using the $2^{-\Delta\Delta Ct}$ method. Gene expression levels were normalized to *ACTB*.

Western blotting analysis

Total proteins were extracted using RIPA lysis buffer (Beyotime, China) with protease inhibitors cocktail (Roche Diagnostics, Basel, Switzerland). Then, equal amounts of protein lysates were run on 10% SDS-PAGE, and the separated bands were transferred to polyvinylidene fluoride membrane (PVDF; EMD Millipore, Billerica, MA, USA). The membranes were blocked with 5% non-fat dried milk for 1 h at room temperature, and then were incubated with

primary antibodies against RPA3 (1:1000, ab97436, Abcam, Cambridge, MA, USA), YY1 (1:5000, ab245365, Abcam), γ-H2AX (1:5000, ab11174, Abcam) and β-Actin (1:5000, ab179467, Abcam) overnight at 4°C, followed by incubation with horseradish peroxidase (HRP)-conjugated secondary antibody for 1 h at room temperature. The protein bands were visualized using ECL detection reagent (Millipore, Billerica, MA, USA).

Clonogenic assay

Clonogenic survival assay was conducted following one previous protocol (Franken *et al.*, 2006). Cells transfected with RPA3 siRNA or scrambled control were seeded into 6-well plates. After adhesion, they were irradiated at defined doses (0, 2, 4, 6, or 8 Gy), using a Rad Source R2000 X-ray irradiator (1.1 Gy/min., 160 kV, 25 mA, 0.3 mm copper filters, Rad Source Tech, Suwanee, GA, USA). After 7–14 days of incubation, the cultures were fixed with 100% methanol and then stained with 1% crystal violet. Colonies containing >50 cells were counted by microscopic inspection. The plating efficiency (PE) of un-irradiated cells (0 Gy) was calculated by the formula: PE = number of colonies counted/number of cells plated. The surviving fraction (SF) of the irradiated cells was calculated using the formula: SF = number of colonies formed after treatment/number of cells seeded × PE. A linear-quadratic model was utilized to generate survival curves using the following equation (Bodgi and Foray, 2016): $Y = e^{(-1 \times (A \times X + B \times X2))}$, in which Y is the fraction survival, and X is the dose. A equals (−1)-times the initial slope, and the initial value of B equals (−0.1)-times the initial slope.

Immunofluorescence assay

MDA-MB-231 and SK-BR-3 cells with or without inhibition of endogenous *RPA3* were seeded in 24-well plates and exposed to 6 Gy of irradiation. 24 h later, the cells were fixed in 4% paraformaldehyde, permeabilized in 0.1% Triton X-100 and blocked using 10% goat serum. Then, the cells were incubated with the primary antibody against γ-H2AX (ab11174, Abcam). After that, the cells were incubated with a secondary antibody conjugated to fluorescein isothiocyanate. DAPI was used for nuclear staining. γ-H2AX foci were visualized under a fluorescence microscope (Olympus IX71, Tokyo, Japan). Five random fields were examined to estimate the number of foci per cell for each coverslip.

Chromatin immunoprecipitation (ChIP)-qPCR

ChIP was performed using the Chromatin Immunoprecipitation Kit (17-295, Merck Millipore, Boston, MA, USA) according to the recommended protocol. Briefly, formaldehyde was used to cross-link the proteins to the DNA. The lysates of MDA-MB-231 and SK-BR-3 cells were sonicated to shear DNA to an average fragment size of 200–1000 bp. Then, samples were pre-cleaned with Protein A Agarose/Salmon Sperm DNA (50% Slurry) (Catalog #16-157C) and subsequently incubated with anti-YY1 (ab245365, Abcam) or IgG antibodies overnight at 4°C with rotation. Immunoprecipitated DNA was collected by adding the previously mentioned Protein A beads. Then, the samples were washed, and DNA levels were measured by qPCR. Three primer sets were designed (Tab. 1), among which two sets covered potential YY1 binding sites (−998 ~ −882/−884 ~ −808) (primer set 1 and 2, Tab. 1) and one set of primers not covering YY1 binding site (−22 ~ +73) (set 3, Tab. 1).

Dual-luciferase assay

Full length and truncated 5' flanking sequences of *RPA3* promoter, including −900/+277, −800/+277, and −150/+277, were cloned into the pGL3-basic plasmid (Promega, Madison, WI, USA). MDA-MB-231 cells were seeded in 24-well plates (2×10^5 cells per well). 24 h later, the cells were transfected with either 1 μg recombinant vectors with different fragments of *RPA3* promoter together with 50 nM YY1 siRNA or scramble control, using Lipofectamine 2000 (Invitrogen). 0.05 μg of the pRL-CMV vector was co-transfected to normalize the transfection efficiency. 24 h later, the cells were lysed for measuring luciferase activity, using a dual-specific luciferase assay kit (#E1910, Promega).

Statistical analysis

Welch's unequal variances t-test was performed for two-group comparison. A Log-rank test was performed for comparing Kaplan-Meier survival curves. Pearson's correlation r was calculated for correlation assessment. $p < 0.05$ was considered statistically significant.

Results

In silico analysis of RPA3 expression profile and prognostic value in breast cancer

RNA-seq data from GTEx-normal mammary tissue and TCGA-BRCA showed that normal mammary tissue owned

TABLE 1

Primers for ChIP-qPCR assay

Primer set	Type	Sequence	Start	Amplicon length
Set 1	Forward Primer	CCTAGCATCATCAGATCCACAG	−22	96
Set 1	Reverse Primer	ATGTGTGTTGTCCTCCTTCTC	73	
Set 2	Forward Primer	GCTCAGAGGCAAGTTGAAGA	−884	77
Set 2	Reverse Primer	CAAGCCCACATGAGAGTGTAG	−808	
Set 3	Forward Primer	GAAATCCCTTGTGAGACTCTACTG	−966	85
Set 3	Reverse Primer	AGCAGGTGATGGTGATGATG	−882	

the lowest *RPA3* expression (Fig. 1A). Tumor adj. normal and all PAM50 subtypes of breast tumors presented elevated *RPA3* expression (Fig. 1A). IHC staining in the HPA confirmed RPA3 expression at the protein level in breast cancer tissues (Fig. 1B). Then, we assessed the survival difference between patients with high (top 50%) and low (bottom 50%) *RPA3* expression in luminal A, luminal B, HER2$^+$, and basal-like subgroups, respectively, using survival data from TCGA-BRCA. The log-rank test indicated that in patients with HER2$^+$ tumors, the high *RPA3* expression group had significantly worse PFS and DSS ($p < 0.05$, Figs. 1E and 1I). The high *RPA3* expression basal-like tumor group was also associated with significantly shorter PFS ($p = 0.024$) and tended to have worse DSS ($p = 0.057$) (Figs. 1F and 1J). However, no survival difference was observed in luminal A and B cases by median *RPA3* stratification (Figs. 1C, 1D, 1G and 1H).

To validate the survival difference, we also checked survival data in the Kaplan-Meier Plotter. Under both median and optimal *RPA3* expression cutoff models, high *RPA3* expression HER2$^+$ cases had significantly worse RFS (Suppl. Figs. 1A and 1B). In basal-like cases, high *RPA3* expression-associated worse RFS was confirmed under the optimal cutoff model (Suppl. Fig. 1D), but not in the median expression model (Suppl. Fig. 1C).

In silico analysis of the correlation between RPA3 expression and functional states of basal-like and HER2$^+$ tumor cells

Using cellular functional states assessed by the CancerSea, we analyzed the correlation between *RPA3* expression and 14 functional states of basal-like (N = 89) and HER2$^+$ tumor cells (N = 130) in GSE75688. Correlation analysis indicated that *RPA3* expression was positively correlated with cell cycle progression, DNA damage, and DNA repair in both basal-like and HER2$^+$ tumor cells (Pearson's r ≥ 0.2, Fig. 2A).

RPA3 inhibition increased the radiosensitivity of basal-like and HER2$^+$ breast cancer cells

MDA-MB-231 and SK-BR-3 cells were transfected with *RPA3* siRNA (Figs. 2B and 2C). Compared with the scramble group, the survival fractions of siRPA3 transfected MDA-MB-231 (Fig. 2D) and SK-BR-3 (Fig. 2E) cells were dramatically decreased after irradiation. Besides, siRPA3 treatment also increased the number of γ-H2AX foci (Figs. 2F–2H) and γ-H2AX expression 24 h after irradiation in both MDA-MB-231 and SK-BR-3 cells (Figs. 2I and 2J). These results suggested that *RPA3* inhibition enhanced the radiosensitivity of basal-like and HER2$^+$ breast cancer cells.

RPA3 expression was transcriptionally activated by YY1 in basal-like and HER2$^+$ breast cancer cells

To explore the mechanisms underlying *RPA3* dysregulation, we assessed the correlation between the expression of transcriptional factors (TFs) in the JASPAR database (N = 669) and *RPA3* in basal-like and HER2$^+$ tumors, respectively (Fig. 3A). Correlation analysis (Suppl. Tab. 1) indicated that among the 669 TFs, only *YY1* was moderately and positively correlated (|Pearson's r| ≥ 0.4) with *RPA3*

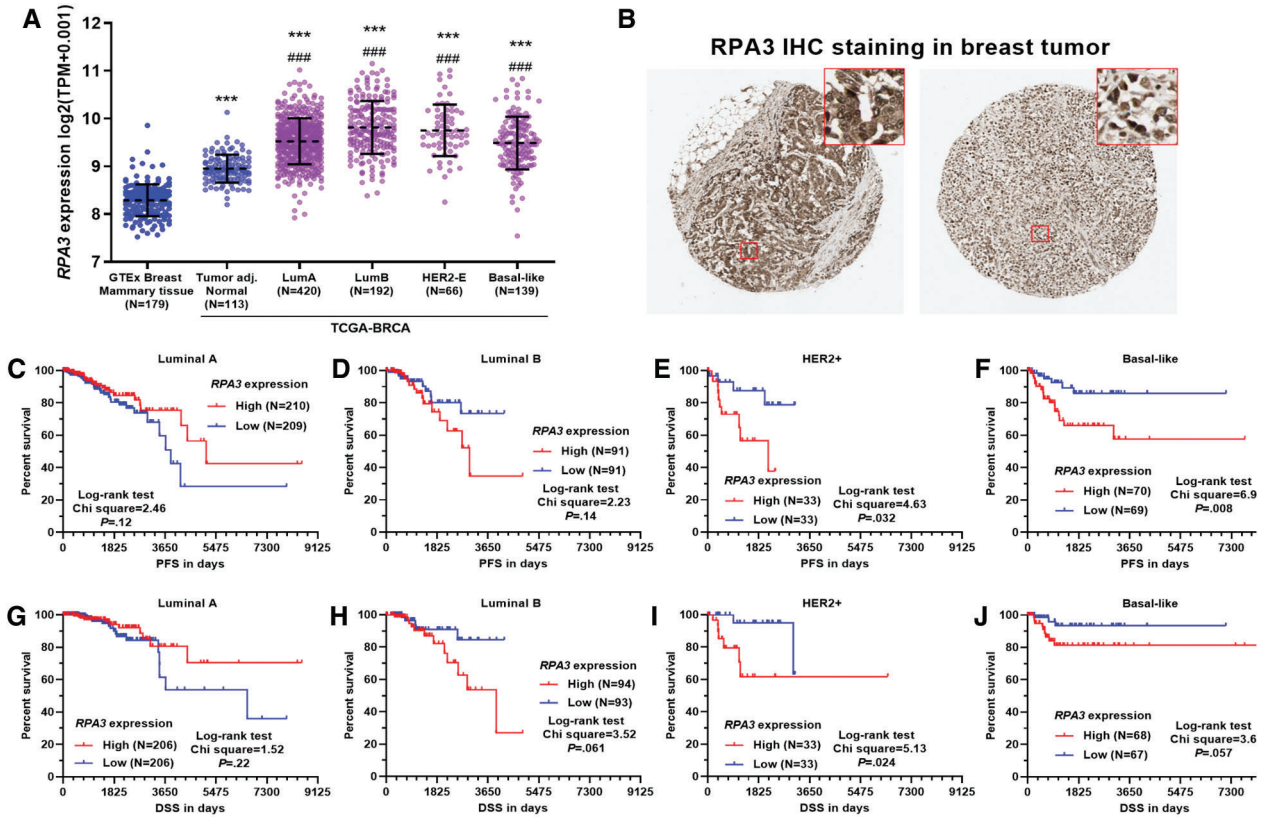

FIGURE 1. High *RPA3* expression was associated with poor survival of basal-like and HER2$^+$ breast cancer.
(A) Comparison of RPA3 expression in normal mammary tissue in GTEx (N = 179), breast cancer adj. normal tissues (N = 113) and the four major PAM50 subtypes in TCGA-BRCA. **(B)** IHC staining of RPA3 expression in breast cancer tissues. Image credit: Human Protein Atlas, from: https://www.proteinatlas.org/ENSG00000106399-RPA3/pathology/breast+cancer#img. **(C–J)** Kaplan-Meier survival analysis of PFS (C–F) and DSS (G–J) in patients with luminal A (C and G), luminal B (D and H), HER2$^+$ (E and I) and basal-like (F–J) tumors in TCGA-BRCA. Patients were grouped by median *RPA3* expression. $^{***}p < 0.001$, compared to GTE-normal mammary tissue group; $^{###}p < 0.001$, compared to tumor adj. normal group.

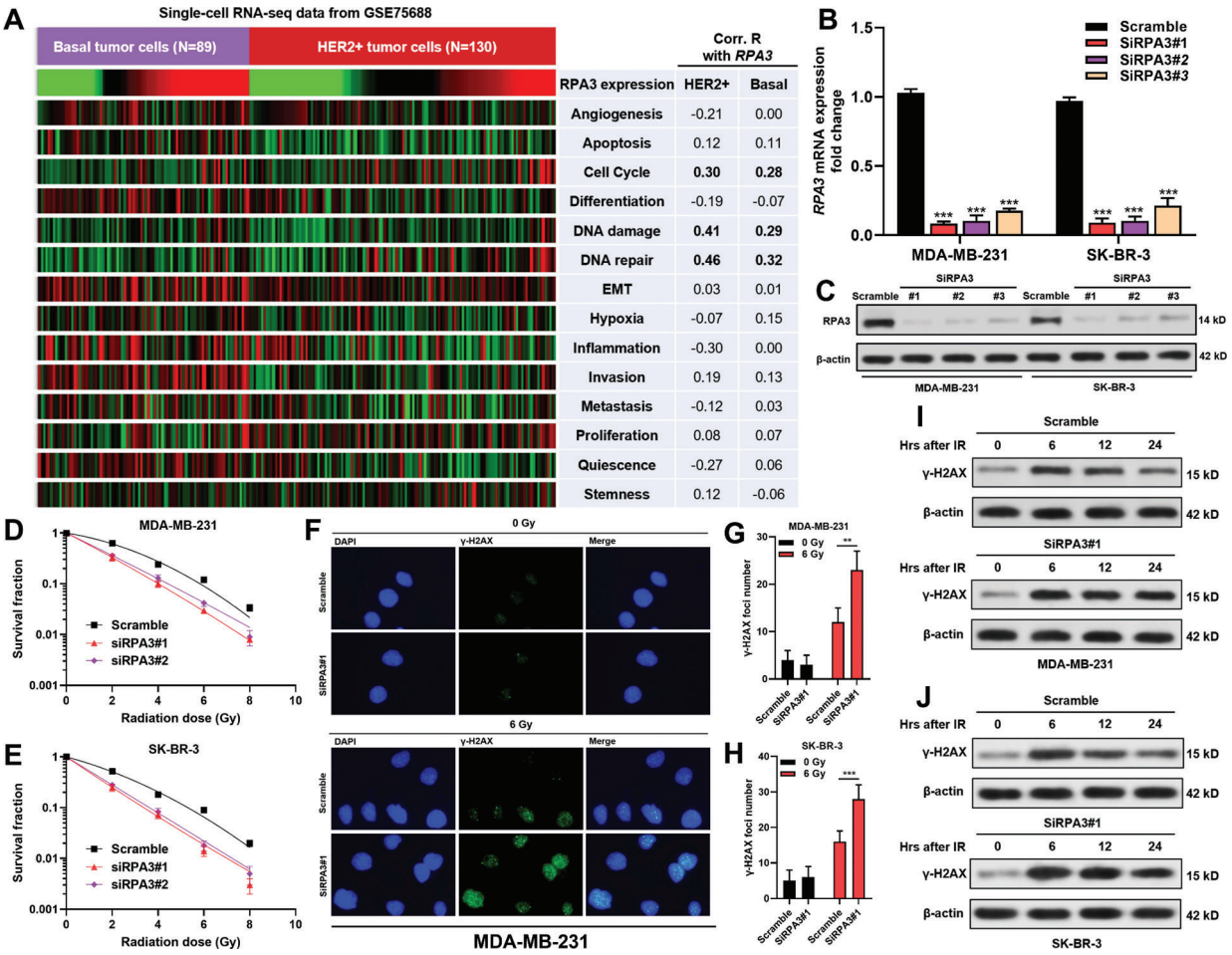

FIGURE 2. *RPA3* inhibition increased radiosensitivity of basal-like and HER2$^+$ breast cancer cells.
(A) Heatmap (left) and summary table (right) showing the correlation between *RPA3* expression and 14 cellular states in basal-like and HER2$^+$ subtypes. The states with |Pearson's r| ≥ 0.2 with *RPA3* expression in both subtypes were highlighted in bold font. **(B–C)** RT-qPCR (B) and western blot (C) analysis of *RPA3* expression in MDA-MB-231 and SK-BR-3 cells 48 h after transfection of 50 nM siRPA3. **(D–E)** Colony formation assay was performed to detect survival fraction in transfected MDA-MB-231 (D) and SK-BR-3 (E) cells with indicated doses of irradiation (0, 2, 4, 6, or 8 Gy). **(F–H)** Representative image (F) and quantitation (G–H) of γ-H2AX foci formation assay in transfected MDA-MB-231 (F–G) and SK-BR-3 (H) cells with 6 Gy irradiation. **(I–J)** Western blotting analysis of γ-H2AX expression in MDA-MB-231 (I) and SK-BR-3 (J) cells transfected with siRPA3#1, at the indicated time points after 6 Gy irradiation.

expression in both basal-like and HER2$^+$ tumor tissue (Suppl. Tab. 1, Figs. 3B and 3C). Via scanning the promoter sequence of *RPA3*, we found five high potential YY1 binding sites (Fig. 3D). YY1 depletion in MDA-MB-231 and SK-BR-3 cells resulted in significantly decreased *RPA3* expression at the mRNA and protein levels (Figs. 3E–3G). Concerning CHIP-qPCR findings, the two amplicons covering YY1 binding sites, but not of the amplicon without YY1 bind site, were significantly enriched upon anti-YY1 immunoprecipitation in both breast cancer cells (Figs. 3H–3I). Dual-luciferase reporter assay showed that the luciferase construct with the integrated promoter sequence had the strongest luciferase activity (Fig. 3J). Truncating the binding sites significantly reduced the luciferase activity (Fig. 3J). YY1 inhibition also substantially decreased the intensity of luciferase expression (Fig. 3J).

In silico analysis of RPA3 and YY1 CNAs

RPA3/YY1 expression and their CNAs in basal-like and HER2$^+$ breast cancer cases in TCGA are shown in Fig. 4A. Correlation analysis indicated that in basal-like cases, the expression of *RPA3* and *YY1* was moderately correlated (Pearson's r ≥ 0.4) with their gene-level copy number (Figs. 4B and 4D). In HER2$^+$ cases, a moderate positive correlation was observed between *YY1* expression and its copy number (Fig. 4E). In comparison, no significant correlation was found between *RPA3* expression and its copy number (Fig. 4C).

Discussion

For patients with basal-like and HER2$^+$ breast tumors, it is now well established that radiation therapy reduces locoregional recurrence rate and provides survival benefits for high-risk patients (He *et al.*, 2018; Liu *et al.*, 2019). However, local recurrence rate improvement of basal-like and HER2$^+$ tumors after radiotherapy is significantly smaller compared to the luminal subtypes (Kyndi *et al.*, 2008), suggesting that these two subtypes are more radioresistant. Therefore, it is meaningful to find new radiosensitization targets to reduce the inherent and induced radiation-resistance. RPA complex members have been

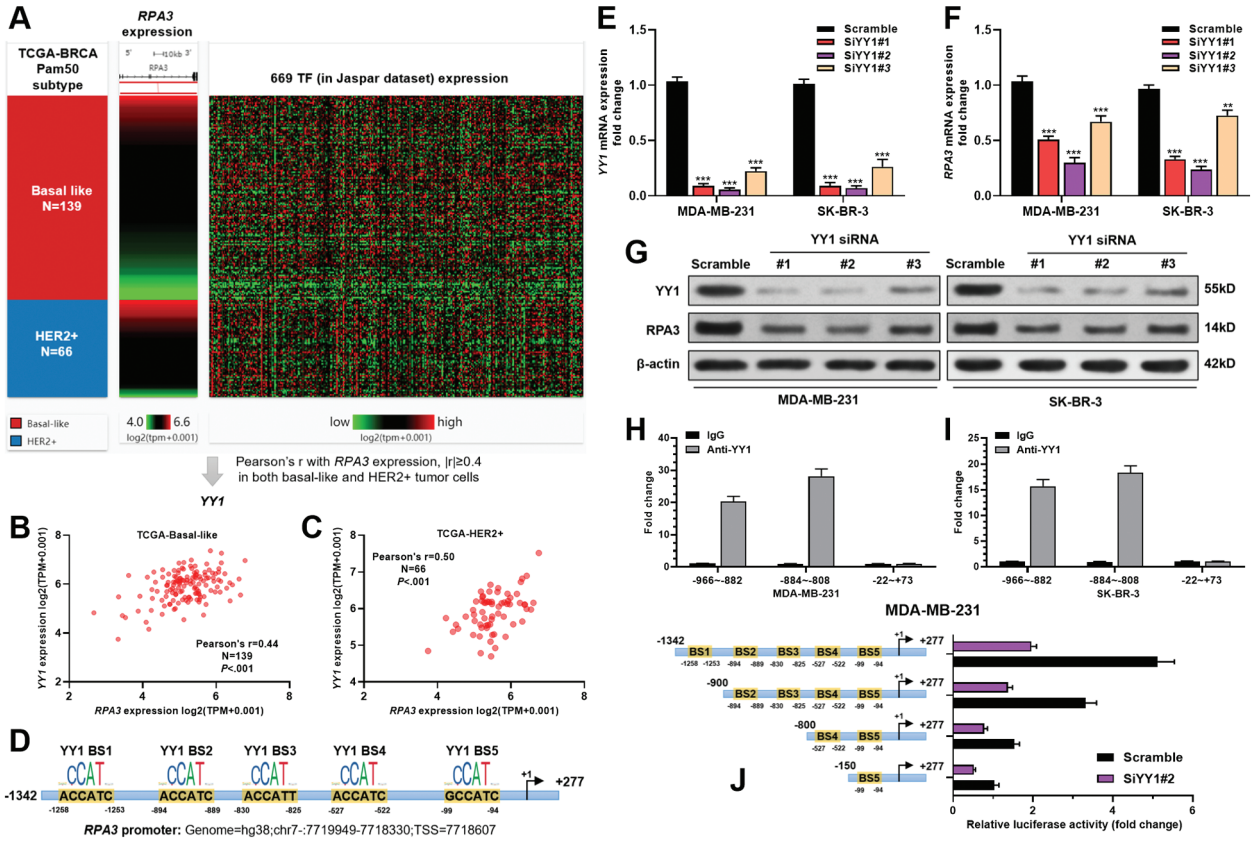

FIGURE 3. *RPA3* expression is transcriptionally activated by YY1 in basal-like and HER2$^+$ breast cancer cells.
(A) A Heatmap showing the correlation between *RPA3* expression and TFs in JASPAR database in basal-like and HER2$^+$ subtypes in TCGA. Correlation analysis was conducted to identify the TFs with moderate correlation with RPA3 expression in both subtypes. **(B–C)** Plot charts showing the correlation between *RPA3* and *YY1* expression in basal-like (B) and HER2$^+$ (C) subtypes, respectively. **(D)** Predicted binding sites of YY1 in the promoter region of *RPA3*. **(E–G)** RT-qPCR (E–F) and western blot (G) analysis of *YY1* and *RPA3* expression in MDA-MB-231 and SK-BR-3 cells 48 h after transfection of 50 nM siYY1. **(H–I)** ChIP-qPCR assays were performed using anti-YY1 and control IgG antibodies in MDA-MB-231 (H) and SK-BR-3 (I) cells. Fold enrichment of the amplicons in the *RPA3* promoter was calculated. **(J)** MDA-MB-231 cells were transfected with different length of reporter constructs, including pGL3-(−1342/+277), pGL3-(−900/+277) (D), and pGL3-(−150/+277), in combination with siYY1#2 or scramble control. 48 h later, luciferase activity was determined.

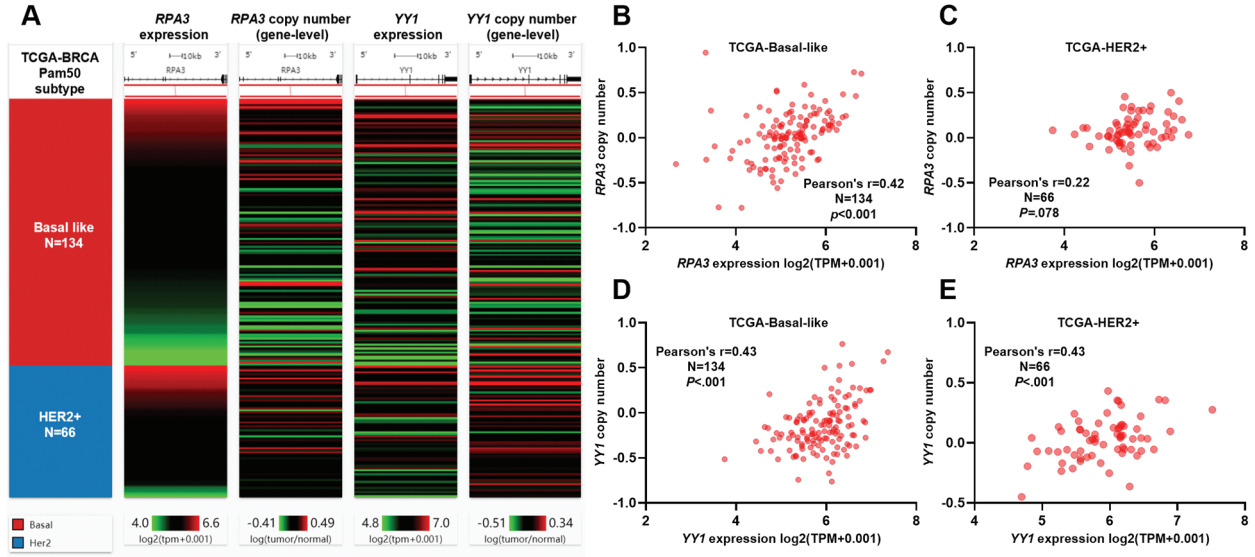

FIGURE 4. Both *RPA3* and *YY1* expression was associated with gene-level copy number.
(A) A Heatmap showing the correlation between gene expression (*RPA3* and *YY1*) and gene-level copy number in basal-like and HER2$^+$ subtypes in TCGA. **(B–E)** Plot charts showing the correlation of *RPA3* and *YY1* expression with their copy in basal-like (B and D) and HER2+ (C and E) subtypes, respectively.

considered as potential targets for radio-sensitization. Previous studies found that silencing *RPA1* reduces the radio-resistance of a hypopharyngeal cancer cell line (Liu *et al*., 2020). *RPA1* or *RPA2* inhibition can induce G2/M arrest and enhance the radiosensitivity of esophageal cancer cells (Zhao *et al*., 2014). Inhibiting *RPA3* expression can sensitize hepatocellular carcinoma (Luo *et al*., 2019) and nasopharyngeal carcinoma (Qu *et al*., 2017) cells to radiation. In this study, we revealed that *RPA3* upregulation was associated with unfavorable survival of basal-like and HER2$^+$ breast cancer. In addition, our *in-vitro* cellular studies demonstrated that inhibiting *RPA3* expression sensitized MDA-MB-231 and SK-BR-3 cells to irradiation. Therefore, *RPA3* might serve as a potential target of radio-sensitization in basal-like and HER2$^+$ breast cancer.

By systemic bioinformatic screening of TFs and *in vitro* studies, we demonstrated that YY1 was an upstream regulator of *RPA3*. YY1 directly bound to the *RPA3* promoter and activated its transcription in MDA-MB-231 and SK-BR-3 cells. A series of studies showed that YY1 acts as an important TF involved in breast cancer development and therapeutic resistance via multiple mechanisms (Sarvagalla *et al*., 2019). YY1 physically interacts with p27 and promotes its ubiquitination, thereby enhancing clonogenicity, migration, invasion, and tumor formation of breast cancer cells (Wan *et al*., 2012). Furthermore, YY1 directly activates heat shock factor 1 (HSF1) transcription to promote transforming growth factor-β (TGFβ)-triggered proliferation and migration of MDA-MB-231 cells (Yang *et al*., 2019). It also reduces miR-873-5p expression by recruiting histone deacetylase 4 (HDAC4) and HDAC9 to the miR-873-5p promoter, thereby activating PI3K/AKT and ERK1/2 pathways and increasing the stemness and chemoresistance of breast cancer cells (Guo *et al*., 2020). YY1 binds to the LINC00673 promoter and suppresses its transcription. Subsequently, LINC00673 acts as a competing endogenous RNA for miR-515-5p, leading to upregulated *MARK4* expression and inhibited Hippo signaling pathway (Qiao *et al*., 2019). Findings in the current study help expand our understanding of the downstream molecular mechanism of YY1 in breast cancer.

Using gene-level copy number alteration data in TCGA, we found that both *RPA3* and *YY1* upregulation was positively correlated with their copy numbers in certain PAM50 subtypes. Some recent studies revealed that therapeutic interventions drive both genetic and epigenetic evolutions of breast cancers (Magnani *et al*., 2017; Nam *et al*., 2020). The genetic alterations favoring cancer cell survival under stressful conditions are more likely to be retained (Nam *et al*., 2020). Since *RPA3* and *YY1* upregulation contributes to breast cancer development and therapeutic resistance, the part of tumor cells with elevated *RPA3* and *YY1* expression might have higher chances to overcome chemo/radiotherapy induced cell death. These findings suggest that the mechanisms leading to *RPA3* dysregulation in breast cancer are multifaceted. Therefore, it is necessary to explore other genetic and epigenetic mechanisms associated with its dysregulation in future studies.

Conclusion

This study revealed that *RPA3* was upregulated in breast cancer and was associated with poor survival and radio-resistance of basal-like and HER2$^+$ breast tumors. Its expression was transcriptionally activated by YY1. It might serve as a potential target for radio-sensitization in basal-like and HER2$^+$ breast cancer.

Availability of data and materials: The datasets analyzed during the current study are available from the corresponding author on reasonable request.

Author Contribution: The authors confirm contribution to the paper as follows: Study conception and design: Yanfei LI, Lulu DAI; data collection: Yanfei LI, Ke CAI; analysis and interpretation of results: Yanfei LI, Yingkui SONG, Xiqing LIU; draft manuscript preparation: Yanfei LI, Xiqing LIU. All authors reviewed the results and approved the final version of the manuscript.

Ethics Approval: Ethics approval is required since no primary data were collected from human or animal tissues in the current study.

Funding Statement: The authors received no specific funding for this study.

Conflicts of Interest: The authors declare that they have no conflicts of interest to report regarding the present study.

References

Aboussekhra A, Biggerstaff M, Shivji MK, Vilpo JA, Moncollin V, Podust VN, Protić M, Hübscher U, Egly JM, Wood RD (1995). Mammalian DNA nucleotide excision repair reconstituted with purified protein components. *Cell* **80**: 859–868. DOI 10.1016/0092-8674(95)90289-9.

Bodgi L, Foray N (2016). The nucleo-shuttling of the ATM protein as a basis for a novel theory of radiation response: Resolution of the linear-quadratic model. *International Journal of Radiation Biology* **92**: 117–131. DOI 10.3109/09553002.2016.1135260.

Consortium GT (2013). The genotype-tissue expression (GTEx) project. *Nature Genetics* **45**: 580–585. DOI 10.1038/ng.2653.

Chung W, Eum H H, Lee HO, Lee KM, Lee HB, Kim KT, Ryu HS, Kim S, Lee JE, Park YH, Kan Z, Han W, Park WY (2017). Single-cell RNA-seq enables comprehensive tumour and immune cell profiling in primary breast cancer. *Nature Communications* **8**: 15081. DOI 10.1038/ncomms15081.

Dai Z, Wang S, Zhang W, Yang Y (2017). Elevated expression of RPA3 is involved in gastric cancer tumorigenesis and associated with poor patient survival. *Digestive Diseases and Sciences* **62**: 2369–2375. DOI 10.1007/s10620-017-4696-6.

Franken NA, Rodermond HM, Stap J, Haveman J, van Bree C (2006). Clonogenic assay of cells *in vitro*. *Nature Protocols* **1**: 2315–2319. DOI 10.1038/nprot.2006.339.

Glanzer JG, Liu S, Wang L, Mosel A, Peng A, Oakley GG (2014). RPA inhibition increases replication stress and suppresses tumor growth. *Cancer Research* **74**: 5165–5172. DOI 10.1158/0008-5472.CAN-14-0306.

Goldman MJ, Craft B, Hastie M, Repečka K, McDade F, Kamath A, Banerjee A, Luo Y, Rogers D, Brooks AN, Zhu J, Haussler D (2020). Visualizing and interpreting cancer genomics data via the Xena platform. *Nature Biotechnology* **38**: 675–678. DOI 10.1038/s41587-020-0546-8.

Guo Q, Wang T, Yang Y, Gao L, Zhao Q, Zhang WZ, Tao X, Zhang LF (2020). Transcriptional factor Yin Yang 1 promotes the stemness of breast cancer cells by suppressing miR-873-5p transcriptional activity (March 3, 2020). *https://ssrn.com/abstract=3531072* or http://dx.doi.org/10.2139/ssrn.3531072.

Gyorffy B, Lanczky A, Eklund AC, Denkert C, Budczies J, Li Q, Szallasi Z (2010). An online survival analysis tool to rapidly assess the effect of 22,277 genes on breast cancer prognosis using microarray data of 1,809 patients. *Breast Cancer Research and Treatment* **123**: 725–731. DOI 10.1007/s10549-009-0674-9.

He MY, Rancoule C, Rehailia-Blanchard A, Espenel S, Trone JC, Bernichon E, Guillaume E, Vallard A, Magné N (2018). Radiotherapy in triple-negative breast cancer: Current situation and upcoming strategies. *Critical Reviews in Oncology/Hematology* **131**: 96–101. DOI 10.1016/j.critrevonc.2018.09.004.

Kyndi M, Sørensen FB, Knudsen H, Overgaard M, Nielsen HM, Overgaard J (2008). Estrogen receptor, progesterone receptor, HER-2, and response to postmastectomy radiotherapy in high-risk breast cancer: The Danish Breast Cancer Cooperative Group. *Journal of Clinical Oncology* **26**: 1419–1426. DOI 10.1200/JCO.2007.14.5565.

Langlands FE, Horgan K, Dodwell DD, Smith L (2013). Breast cancer subtypes: Response to radiotherapy and potential radiosensitisation. *British Journal of Radiology* **86**: 20120601. DOI 10.1259/bjr.20120601.

Lin YL, Shivji MK, Chen C, Kolodner R, Wood RD, Dutta A (1998). The evolutionarily conserved zinc finger motif in the largest subunit of human replication protein A is required for DNA replication and mismatch repair but not for nucleotide excision repair. *Journal of Biological Chemistry* **273**: 1453–1461. DOI 10.1074/jbc.273.3.1453.

Liu C, Liao K, Gross N, Wang Z, Li G, Zuo W, Zhong S, Zhang Z, Zhang H, Yang J, Hu G (2020). Homologous recombination enhances radioresistance in hypopharyngeal cancer cell line by targeting DNA damage response. *Oral Oncology* **100**: 104469. DOI 10.1016/j.oraloncology.2019.104469.

Liu QQ, Sun HF, Yang XL, Chen MT, Liu Y, Zhao Y, Zhao YY, Jin W (2019). Survival following radiotherapy in young women with localized early-stage breast cancer according to molecular subtypes. *Cancer Medicine* **8**: 2840–2857. DOI 10.1002/cam4.2186.

Lu X, Liu R, Wang M, Kumar AK, Pan F, He L, Hu Z, Guo Z (2019). MicroRNA-140 impedes DNA repair by targeting FEN1 and enhances chemotherapeutic response in breast cancer. *Oncogene* **39**: 234–247. DOI 10.1038/s41388-019-0986-0.

Luo J, Si ZZ, Li T, Li JQ, Zhang ZQ, Chen GS, Qi HZ, Yao HL (2019). MicroRNA-146a-5p enhances radiosensitivity in hepatocellular carcinoma through replication protein A3-induced activation of the DNA repair pathway. *American Journal of Physiology-Cell Physiology* **316**: C299–C311. DOI 10.1152/ajpcell.00189.2018.

Magnani L, Frigè G, Gadaleta RM, Corleone G, Fabris S, Kempe H, Verschure PJ, Barozzi I, Vircillo V, Hong SP, Perone Y, Saini M, Trumpp A, Viale G, Neri A, Ali S, Colleoni MA, Pruneri G, Minucci S (2017). Acquired CYP19A1 amplification is an early specific mechanism of aromatase inhibitor resistance in ERα metastatic breast cancer. *Nature Genetics* **49**: 444–450. DOI 10.1038/ng.3773.

Marechal A, Li JM, Ji XY, Wu CS, Yazinski SA, Nguyen HD, Liu S, Jiménez AE, Jin J, Zou L (2014). PRP19 transforms into a sensor of RPA-ssDNA after DNA damage and drives ATR activation via a ubiquitin-mediated circuitry. *Molecular Cell* **53**: 235–246. DOI 10.1016/j.molcel.2013.11.002.

Nam AS, Chaligne R, Landau DA (2020). Integrating genetic and non-genetic determinants of cancer evolution by single-cell multi-omics. *Nature Reviews Genetics* **22**: 3–18. DOI 10.1038/s41576-020-0265-5.

Nielsen T, Wallden B, Schaper C, Ferree S, Liu S, Gao D, Barry G, Dowidar N, Maysuria M, Storhoff J (2014). Analytical validation of the PAM50-based prosigna breast cancer prognostic gene signature assay and nCounter analysis system using formalin-fixed paraffin-embedded breast tumor specimens. *BMC Cancer* **14**: 177. DOI 10.1186/1471-2407-14-177.

Peng G, Chun-Jen LC, Mo W, Dai H, Park YY, Kim SM, Peng Y, Mo Q, Siwko S, Hu R, Lee JS, Hennessy B, Hanash S, Mills GB, Lin SY (2014). Genome-wide transcriptome profiling of homologous recombination DNA repair. *Nature Communications* **5**: 3361. DOI 10.1038/ncomms4361.

Qiao K, Ning S, Wan L, Wu H, Wang Q, Zhang X, Xu S, Pang D (2019). LINC00673 is activated by YY1 and promotes the proliferation of breast cancer cells via the miR-515-5p/MARK4/Hippo signaling pathway. *Journal of Experimental & Clinical Cancer Research* **38**: 418. DOI 10.1186/s13046-019-1421-7.

Qu C, Zhao Y, Feng G, Chen C, Tao Y, Zhou S, Liu S, Chang H, Zeng M, Xia Y (2017). RPA3 is a potential marker of prognosis and radioresistance for nasopharyngeal carcinoma. *Journal of Cellular and Molecular Medicine* **21**: 2872–2883. DOI 10.1111/jcmm.13200.

Sarvagalla S, Kolapalli SP, Vallabhapurapu S (2019). The two sides of YY1 in cancer: A friend and a foe. *Frontiers in Oncology* **9**: 1230. DOI 10.3389/fonc.2019.01230.

Stormo GD (2013). Modeling the specificity of protein-DNA interactions. *Quantitative Biology* **1**: 115–130. DOI 10.1007/s40484-013-0012-4.

Tuo YL, Li XM, Luo J (2015). Long noncoding RNA UCA1 modulates breast cancer cell growth and apoptosis through decreasing tumor suppressive miR-143. *European Review for Medical and Pharmacological Sciences* **19**: 3403–3411.

Vlashi E, Lagadec C, Vergnes L, Reue K, Frohnen P, Chan M, Alhiyari Y, Dratver MB, Pajonk F (2014). Metabolic differences in breast cancer stem cells and differentiated progeny. *Breast Cancer Research and Treatment* **146**: 525–534. DOI 10.1007/s10549-014-3051-2.

Wan M, Huang W, Kute TE, Miller LD, Zhang Q, Hatcher H, Wang J, Stovall DB, Russell GB, Cao PD, Deng Z, Wang W, Zhang Q, Lei M, Torti SV, Akman SA, Sui G (2012). Yin Yang 1 plays an essential role in breast cancer and negatively regulates p27. *American Journal of Pathology* **180**: 2120–2133. DOI 10.1016/j.ajpath.2012.01.037.

Xiao W, Zheng J, Zhou B, Pan L (2018). Replication Protein A 3 is associated with hepatocellular carcinoma tumorigenesis and poor patient survival. *Digestive Diseases* **36**: 26–32. DOI 10.1159/000478977.

Yang W, Feng B, Meng Y, Wang J, Geng B, Cui Q, Zhang H, Yang Y, Yang J (2019). FAM3C-YY1 axis is essential for TGFbeta-promoted proliferation and migration of human breast

cancer MDA-MB-231 cells via the activation of HSF1. *Journal of Cellular and Molecular Medicine* **23**: 3464–3475. DOI 10.1111/jcmm.14243.

Yuan H, Yan M, Zhang G, Liu W, Deng C, Liao G, Xu L, Luo T, Yan H, Long Z, Shi A, Zhao T, Xiao Y, Li X (2019). CancerSEA: A cancer single-cell state atlas. *Nucleic Acids Research* **47**: D900–D908. DOI 10.1093/nar/gky939.

Yusufzai T, Kong X, Yokomori K, Kadonaga JT (2009). The annealing helicase HARP is recruited to DNA repair sites via an interaction with RPA. *Genes & Development* **23**: 2400–2404. DOI 10.1101/gad.1831509.

Zhao D, Sun SY, Lu H, Yu DH (2014). Enhanced radiosensitivity and G2/M arrest were observed in radioresistant esophageal cancer cells by knocking down RPA expression. *Cell Biochemistry and Biophysics* **70**: 887–891. DOI 10.1007/s12013-014-9995-3.

Zou L, Elledge SJ (2003). Sensing DNA damage through ATRIP recognition of RPA-ssDNA complexes. *Science* **300**: 1542–1548. DOI 10.1126/science.1083430.

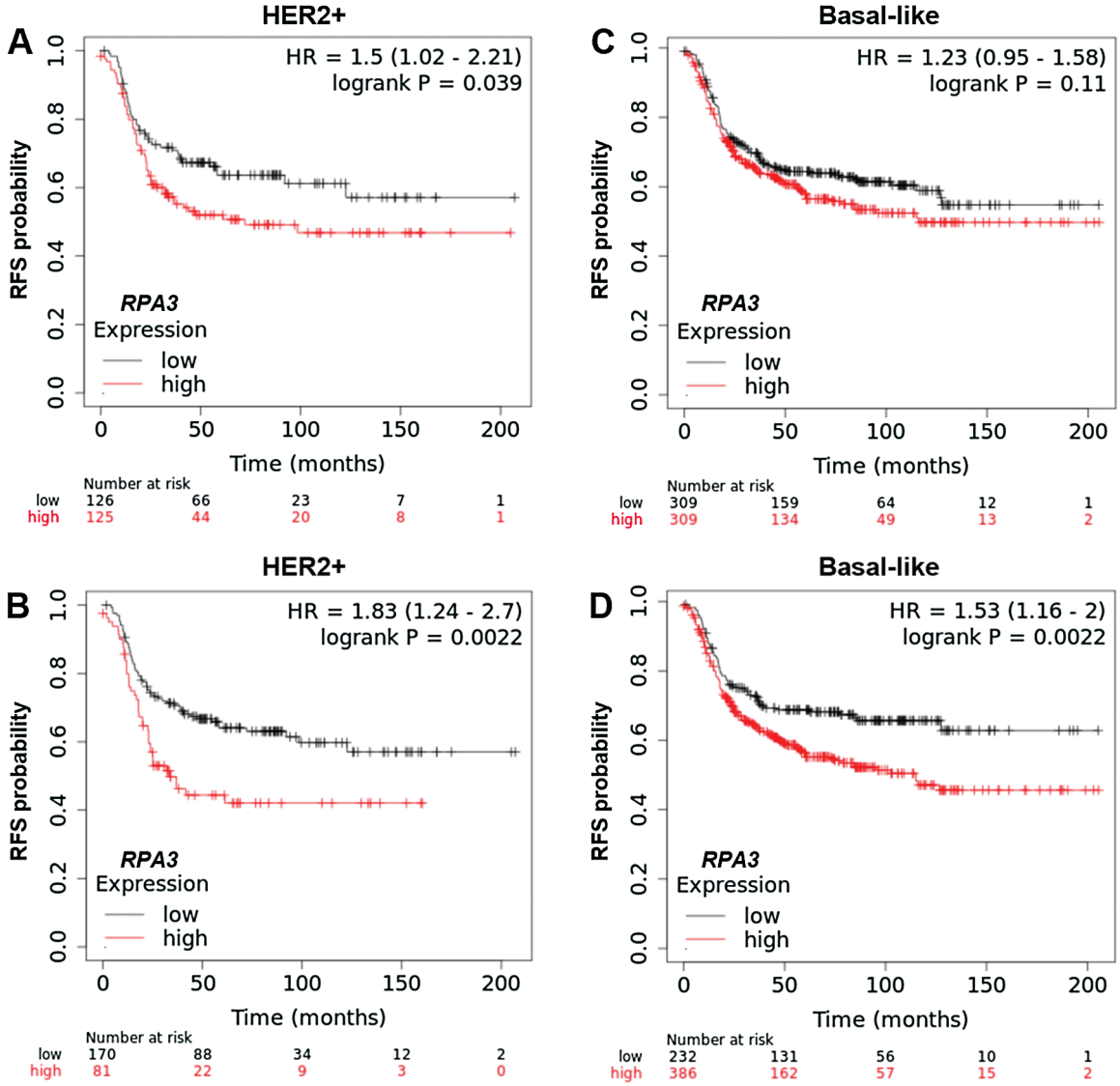

SUPPLEMENTARY FIGURE 1. Kaplan-Meier survival analysis of RFS in Kaplan-Meier Plotter.
(A–D) Kaplan-Meier survival analysis of RFS in patients with HER2$^+$ (A–B) and basal-like (C–D) tumors in Kaplan-Meier Plotter. Patients were grouped by the median (A–B) or the optimal cutoff (C–D) of *RPA3* expression.

SUPPLEMENTARY TABLE 1

TF genes positive correlated with RPA3 (Pearson'r > 0.2) in TCGA-BRCA

Sample type	Correlation with RPA3	
PAM50Call_RNAseq	Basal-like	HER2+
ZNF143	0.34	0.21
YY1	0.44	0.50
NKX3-1	0.21	0.25
CTCF	0.40	0.26
NFE2L2	0.39	0.28
BHLHE40	0.28	0.21
CEBPB	0.26	0.27
E2F6	0.31	0.39
RFX1	0.38	0.22
ZNF263	0.32	0.24
IRF2	0.25	0.31
TFDP1	0.27	0.31
PBX3	0.23	0.24
NFE2L1	0.30	0.33
NR2F6	0.28	0.38
SREBF1	0.23	0.22
ELF4	0.33	0.21
KLF3	0.26	0.22
SP3	0.27	0.21
SP4	0.26	0.28
TFE3	0.32	0.27
THAP11	0.43	0.29
YY2	0.24	0.29
ZNF140	0.22	0.28
ZNF282	0.28	0.23
ZNF75D	0.36	0.28
ATF2	0.21	0.26
ZBTB14	0.27	0.24
ZKSCAN5	0.35	0.24